Measurement of the Local and Non-Local Amplitudes in $B^{\pm} \to K^{\pm}\mu^{\pm}\mu^{\mp}$ Decays at LHCb

Based on arXiv:2603.12477

Zak Williams[1] on behalf of the LHCb Collaboration

16st April 2026 - IGFAE, Santiago de Compostela
Beyond the Flavour Anomalies Workshop 2026

[1]University of Bristol

University of BRISTOL

LHCb

Chapters

Physics Model

- $B^+ \to K^+\mu\mu$ DDR (e.g. [PRD 5 (2016)]) parameterised in $q^2 (\equiv m^2_{\mu\mu})$:
  - $C_A \equiv C_{10} + C'_{10}$ and $C_V \equiv C_9 + C'_9$:
  - $\mathcal{O}_{1-6,7,8}$ absorbed into the vector operator, $\mathcal{O}_V$.

$$\frac{d\Gamma}{dq^2} = \frac{G_F^2\alpha^2\left|V_{tb}V_{ts}^*\right|^2}{2^7\pi^5}|\boldsymbol{k}|\beta\left\{\frac{2}{3}|\boldsymbol{k}|^2\beta^2\left|C_A f_+(q^2)\right|^2 + \frac{m_\mu^2\left(m_B^2-m_K^2\right)^2}{q^2 m_B^2}\left|C_A f_0(q^2)\right|^2 + |\boldsymbol{k}|^2\left[1-\frac{\beta^2}{3}\right]\left|C_V f_+(q^2) + 2\left(C_7 + C'_7\right)\frac{m_b+m_s}{M_B+M_K}f_T(q^2)\right|^2\right\}$$

- C_V, C_A *would* be almost fully degenerate, however:
  - $C_7 + C'_7$ is fixed to the SM [EPJC 5 (2024)], as it is strongly constrained by radiative decays [JHEP 4 (2017)].
  - Non-local fit maximises information in q^2 tail regions, where shape degeneracy breaks.

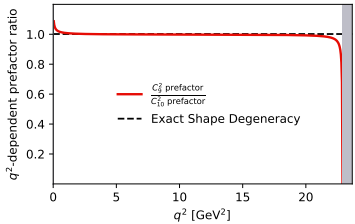

- QCD Form factors (FFs), $f_X(q^2)$, sourced from the HPQCD [PRD 1 (2023)] and FNAL/MILC collaborations [PRD 2 (2016)].

Non-Local Modelling - Method

- Substantial non-local effects present in the form of $q\bar{q}$, $D\bar{D}$ loops.
- Non-local effects modelled with dispersion relations [EPJC 12 (2020)], added to C_9:
  - Strong phase (δ), width (Γ_{0r}), and magnitude (η_r) floated in the fit.
- Full-spectrum unbinned fit allows us to maximally exploit the q^2 shape:
  - Probe potential q^2 dependence of C_9.
  - Shape information is not limited by measurement of normalisation mode $BF(B^+ \to J/\psi K^+)$

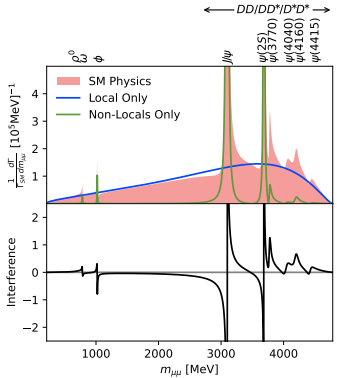

$$C_9 \to C_9^{\text{eff}}(q^2) = C_9 + \sum_r Y_r(q^2, m_r, \delta_r, \eta_r, \Gamma_{0r})$$

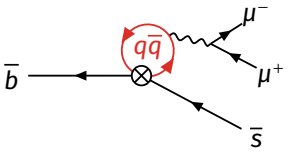

1P ($q\bar{q}$) State

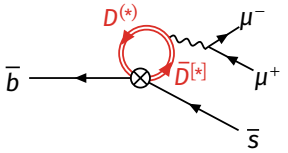

2P ($D\bar{D}$) State

Non-Local Modelling - Suitability

- The capability of this dispersion-like non-local model has been demonstrated in the corresponding $B^0 \to K^{*0}\mu\mu$ analysis [JHEP 5 (2025)].
  - [JHEP 5 (2025)] also favours a value of $\delta C_9^{\text{NP}} < 0$.
  - Measurement of strong-phase-dependent observables (S_7, S_8, S_9...) in [JHEP 5 (2025)] matches values measured in the binned analysis [PRL 1 (2020)].
  - ✔ Dispersion-like non-local model can explain anomalies in binned observables while continuing to observe the C_9 anomaly.

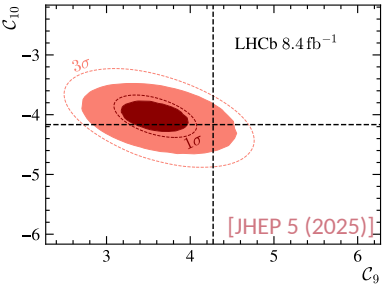

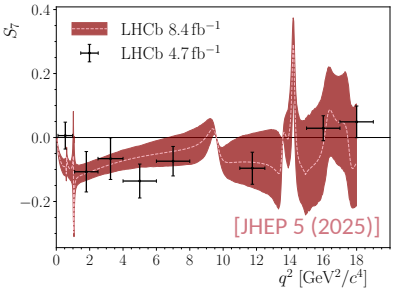

Chapters

Data Selection and Yield

- 8.4fb^{-1} of data is used from run 1 (2010 – 12) and 2 (2015 – 18) at the LHCb:
  - Initial hardware (L0) trigger relies on presence of a high-p_T muon.
  - HLT (software) triggers and offline selection further filters data.
  - PID cuts and BDTs target mis-ID and combinatorial background respectively.
- Yields are fit in 3 $m_{\mu\mu}$ regions, dominated by rare, J/ψ, and $\psi(2S)$ modes:

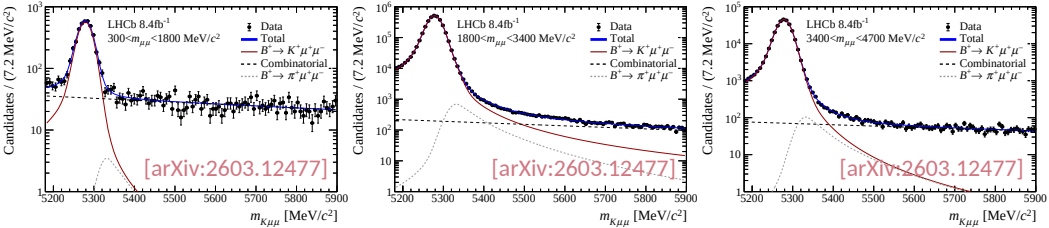

Signal Yield	$\pi \to K$ mis-ID Yield	Combinatorial Yield
$(3.359 \pm 0.002) \times 10^6$	$(3.3 \pm 0.2) \times 10^3$	$(1.6 \pm 0.1) \times 10^3$

Fitter

- Fit parameters obtained by an unbinned NLL fit of model $P\left(m^{\text{rec}}_{\mu\mu}, C_9, C_{10}, ...\right)$ to the data.

where:

$$P(m^{rec}_{\mu\mu}, C_9, C_{10}, ...) = \mathcal{R}(m^{\text{rec}}_{\mu\mu}, m_{\mu\mu}) \otimes \left[2m_{\mu\mu} \frac{dG}{dq^2}(q^2, C_9, C_{10}, ...)\Big|_{\text{eff}} \right] + \\ + P^{\text{combi.}}_{\text{bkg}}(m^{\text{rec}}_{\mu\mu}) + P^{\pi\to K}_{\text{bkg}}(m^{\text{rec}}_{\mu})$$

with: $m_{\mu\mu} \equiv m^{\text{true}}_{\mu\mu}$, $q^2 \equiv {q^2}^{\text{true}}$

- $\mathcal{R}(m^{\text{rec}}_{\mu\mu}, m_{\mu\mu})$: Detector resolution model.
- $\frac{dG}{dq^2}(q^2, C_9, C_{10}, ...)$: Efficiency-modified physics model.
- $P^{\text{combi.}}_{\text{bkg}}(m^{\text{rec}}_{\mu\mu}), P^{\pi\to K}_{\text{bkg}}(m^{\text{rec}}_{\mu\mu})$: Combinatorial and mis-ID background models.

Detector Efficiencies

- Physics-level DDR $d\Gamma/dq^2$ is an integrated form of $d^2\Gamma/dq^2\cos\theta_\mu$:
  - Terms have different efficiency shapes in q^2 based on their $\cos\theta_\mu$ distribution:

$$\left.\frac{dG}{dq^2}\right|_{eff} = \frac{G_F^2\alpha^2\left|V_{tb}V_{ts}^*\right|^2}{2^7\pi^5}|\boldsymbol{k}|\beta\left\{\frac{2}{3}|\boldsymbol{k}|^2\beta^2\left|C_A f_+(q^2)\right|^2\varepsilon_{+C_A}(q^2) + \frac{m_\mu^2\left(m_B^2-m_K^2\right)^2}{q^2 m_B^2}\left|C_A f_0(q^2)\right|^2\varepsilon_{0C_A}(q^2) + |\boldsymbol{k}|^2\left[1-\frac{\beta^2}{3}\right]\left|C_V f_+(q^2) + 2\left(C_7+C_7'\right)\frac{m_b+m_s}{M_B+M_K}f_T(q^2)\right|^2\varepsilon_{+C_V}(q^2)\right\}$$

- Each term is modelled with a 4th-order polynomial in $m_{\mu\mu}$, fit to simulation.
- Simulation is corrected using comparison to high-purity data channels.

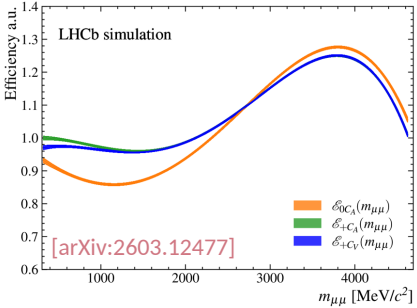

Resolution Model

- J/ψ, $\psi(2S)$, and ϕ have decay widths $\lesssim$ detector resolution in q^2.
  - Detector resolution has a substantial effect on the q^2 shape near large resonances.
- Resolution improved by mass constraint $m_{K\mu\mu} \to m_B^{\mathrm{PDG}}$, but still needs modelling.
  - Modelled by convolving dG/dq^2 with $\mathcal{R}$ in 3 separate $m_{\mu\mu}$ regions.
  - Each window's $\mathcal{R}$ is modelled as a double crystal-ball (DCB) + Gaussian.
  - J/ψ and $\psi(2S)$ window parameters are floated in data, ϕ is fixed in simulation.

$\phi(1020)$ Window
$m_{\mu\mu} \in [300, 1800]$MeV

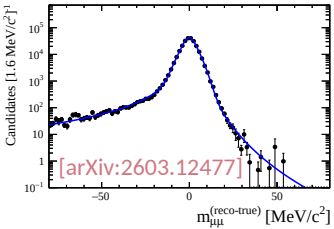

J/ψ Window
$m_{\mu\mu} \in [1800, 3400]$MeV

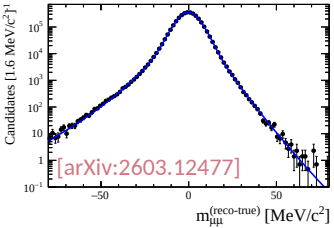

$\psi(2S)$ Window
$m_{\mu\mu} \in [1800, 4700]$MeV

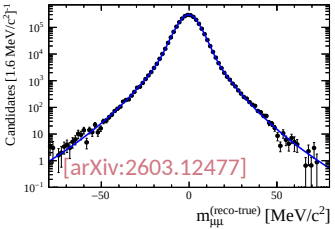

Modelled Backgrounds - Combinatorial

- Resolution-improving contraint on $m_{K\mu\mu}$ distorts the combinatorial background.
  - Distortion is in an $m_{K\mu\mu}$ variant manner.
  - Cannot simply translate the background from high mass regions into the signal window.
- To model the combinatorial in the signal window $\left(|m_{K\mu\mu} - m_B^{\mathrm{PDG}}| < 40\mathrm{MeV}\right)$:
  1. Upper mass side band (UMSB) is split into 5 regions of 80MeV each.
  2. $m_{K\mu\mu}$ in each region is constrained to the central window value.
  3. Analytic function (ARGUS + 2 Gauss on J/ψ + 1 gauss on $\psi(2S)$) fit in each window.
  4. Fit parameters are linearly extrapolated backward to predict values in the fit window.

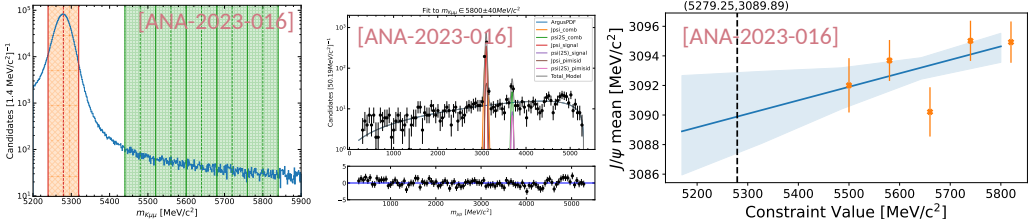

Left: The fiting window and the 5 UMSB windows. Middle: Analytic model fitting to the right-most UMSB window. Right: Linear extrapolation of a combinatorial descriptive parameter, J/ψ peak mean position.

Chapters

J/ψ, $\psi(2S)$ Phase Degeneracy

- 4 separated near-degenerate points in $-2\log\mathcal{L}_{\text{min}}$ are observed across the fit space:
  - Split by −ve or +ve status of J/ψ, $\psi(2S)$ phases. Also true in the previous analysis [EPJC 3 (2017)].
  - $\text{sign}(\delta_{J/\psi}, \delta_{\psi(2S)}) = (-,+)$ has the lowest $-2\mathcal{L}_{\text{min}}$.
  - Choice has a negligible effect on the WC measurements.

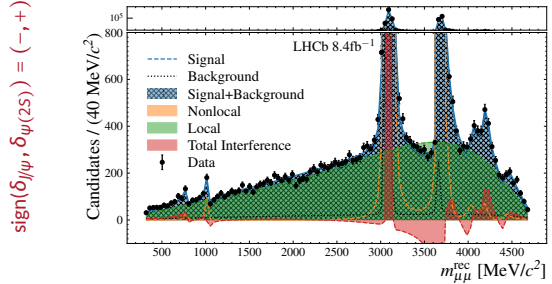

[arXiv:2603.12477]

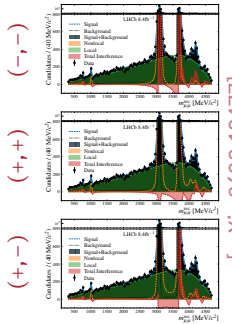

[arXiv:2603.12477]

Value	(−, +)	(+, +)	(−, −)	(+, −)
$\delta_{J/\psi}$	−1.56 ± 0.06 ± 0.01	1.60 ± 0.05 ± 0.01	−1.70 ± 0.07 ± 0.01	1.45 ± 0.04 ± 0.01
$\delta_{\psi(2S)}$	2.21 ± 0.16 ± 0.01	1.77 ± 0.13 ± 0.01	−2.02 ± 0.13 ± 0.01	−2.46 ± 0.11 ± 0.01
$-2\Delta\log\mathcal{L}_{\text{min}}$	0	0.09	0.69	0.463
$\lvert\Delta C_V\rvert$	0	0.006	0.006	0.014
$\lvert\Delta C_A\rvert$	0	0.001	0.011	0.012

dBF/dq^2 Cross Check

- Binned dBF/dq^2 is calculated based on the unbinned fit model.
- A comparison is made with the model-independent dBF/dq^2 measurement on run 1 data [JHEP 6 (2014)].
  - A strong agreement is seen between our model-dependent and the previous dBF/dq^2 measurement.
  - This previous analysis found a suppression in dBF/dq^2 at low q^2.
- Interference observed between the rare and $J/\psi/\psi(2S)$ modes is small.

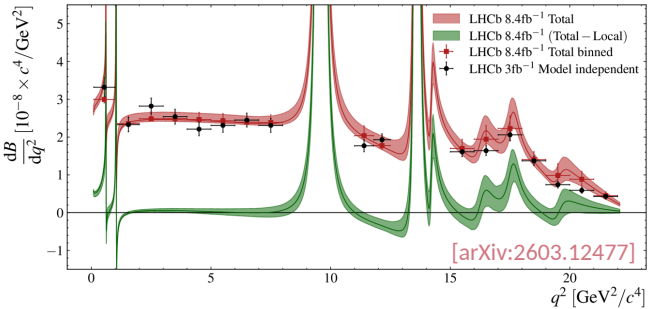

$C_A - C_V$ Fit Plane

- C_V and C_A features a degeneracy valley as a segment of the circlular $C_V^2 + C_A^2 \sim R_0^2$.
- A 4.0σ tension is observed with the SM, when fitting with HPQCD FFs.
  - When performing the same fit using the less precise FNAL/MILC FFs, the fit point remains the same, but the tension is lessened to 1.6σ.
  - Fit valley location is similar to that seen in the run 1 only analysis [EPJC 3 (2017)].

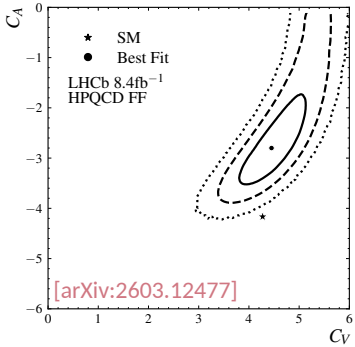

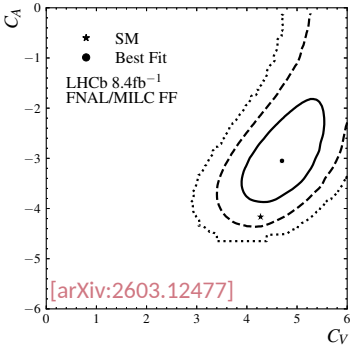

Fit profiles in the (C_V, C_A) plane. Left: Fit using the most recent HPQCD FFs [PRD 1 (2023)]. Right: using the FNAL/MILC FFs. Contours show uncertainties of 68.3%, 95.4%, 99.7% respectively, including systematic uncertainties.

Wilson Coefficient Measurement - Separate

- $C_V - C_A$ planes are not obviously supportive of the common global result: $\delta C_9^{\text{NP}} \simeq -1$.
- C_9, C_{10} are additionally individually fit in isolation:
  - Assuming $C_j^{\text{NP}} = 0$ for every other of $j = 9^{(\prime)}, 10^{(\prime)}$.
  - Done with the HPQCD FFs [PRD 1 (2023)].
- $\delta C_9^{\text{NP}} < 0$:
  - Consistent with [JHEP 9 (2022)], however a smaller shift than in [EPJC 5 (2024)].

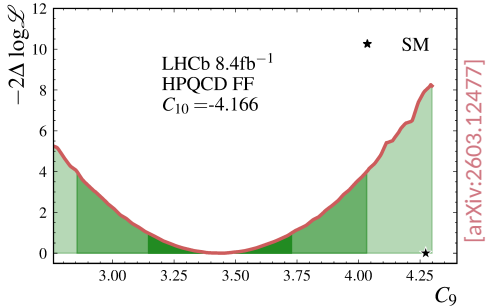

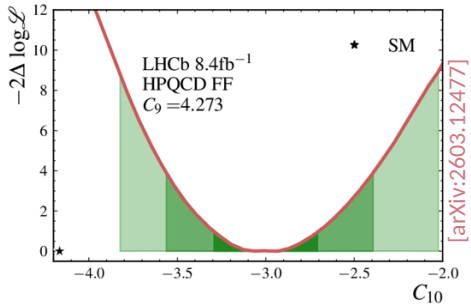

WC Residual q^2 Dependence

- All 3 2P contributions are in P-wave configurations with similar q^2 dependence outside of threshold effects.
- Due to limited statistics, the 3 2P contributions are fit with a common amplitude and strong phase.
  - Despite this measure, There was no evidence of the 2P contribution.
- We trial additional fits with new floating parameters to capture residual q^2 dependencies:

Linear term fit:

$$C_j^{\text{lin}} = C_j + a_j(q^2 - 11.09\text{GeV}^2)$$

Threshold fit:

$$C_V^{\text{thresh}} = C_V + \Delta\left(\frac{e^{x(m_{\mu\mu},m_t)}}{1+e^{x(m_{\mu\mu},m_t)}} - \frac{1}{2}\right) \quad \text{with} \quad x(m_{\mu\mu}, m_t) = \frac{m_{\mu\mu} - m_t}{100\text{MeV}}$$

WC Residual q^2 Dependence - Fit Results

- Linear fits are separately performed for:
  - C_V: $a_V = 0.078 \pm 0.052$
  - C_A: $a_A = -0.090 \pm 0.045$
- Threshold is separately trialled for two m_t values:
  - J/ψ Threshold ($m_t = 3096.65$MeV): $\Delta = 0.41 \pm 0.24$
  - $D\bar{D}^*$ Threshold ($m_t = 3871.70$MeV): $\Delta = -1.37 \pm 0.53$
- Hints at potential q^2 dependence not captured in the current model.
  - Most findicative results are a 2σ linear a_V, and a 2.6σ threshold term at $D\bar{D}^*$.
  - Linear a_A is similar to that obtained in corresponding $B^0 \to K^{*0}\mu\mu$ analysis [JHEP 5 (2025)].
- Variation of systematic uncertainties has a negligible effect on these results.

Chapters

LHCb at Run 3

- LHCb saw substantial upgrades during the shutdown years of 2019-2021.
  - Factor 5 luminosity increase: $4\times10^{32}\text{cm}^{-1}\text{s}^{-1} \rightarrow 2\times10^{33}\text{cm}^{-1}\text{s}^{-1}$.
  - An entirely remade trigger system, including removal of the hardware trigger, increasing signal/luminosity yield.
- ▷ Substantially more statistics available
  - (Re)opens some extra physics goals in the run 3 analysis.
- $B^+ \rightarrow J/\psi(\rightarrow \mu\mu)K^+$ run 3 feasibility analyses are already released [arXiv:2603.12477].

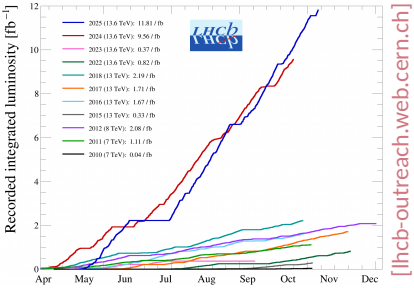

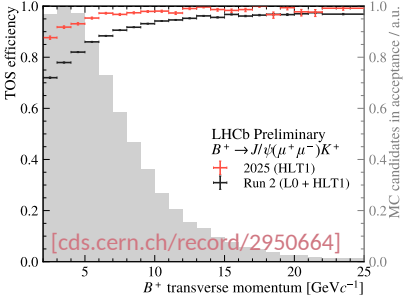

Left: Integrated luminosity in pp collisions at the LHCb. Right: Trigger efficiencies in run 2 and 2025 data at the LHCb.

Run 3 Goal - Multi WC Fit

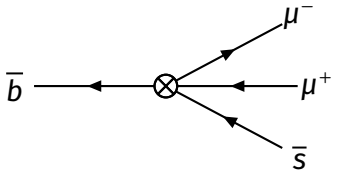

$$\langle \mathrm{f}|\mathcal{H}_{\mathrm{eff}}|\mathrm{i}\rangle = \frac{G_F}{\sqrt{2}} V_{tb} V_{ts}^* \sum_j C_j \langle \mathrm{f}|\mathcal{O}_j|\mathrm{i}\rangle$$

$$j = S^{(\prime)}, P^{(\prime)}, 9^{(\prime)}, 10^{(\prime)}, 7^{(\prime)}_{\mathrm{eff}}, T, T5$$

- In addition to C_V, C_A, and $C_7^{\mathrm{eff}} + C_7'$, the $B^+ \to K^+\mu\mu$ decay is also sensitive to:
  - $C_S + C_S'$, $C_P + C_P'$, C_T, and C_{T5}.
  - These extra WCs are fixed to their SM values (= 0) in the run 1 + 2 fit.
- For greater model independence and to broaden NP search, the run 3 analysis will simultaneously fit for all 6 of these Wilson Coeficients:
  - Also fit for the phases of all but C_{10}, allowing direct CPV.
  - $C_7^{\mathrm{eff}} + C_7'$ remains fixed, as this can be independently determined to a high precision in radiative decays [JHEP 4 (2017)].
  - Continue to use an unreduced form of the physics model described in [PRD 5 (2016)].

Run 3 Goal - C_9^τ

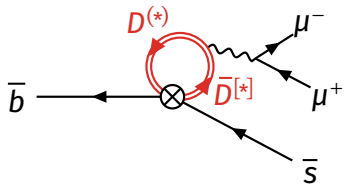

$D^{(*)}\bar{D}^{[*]}$ (2P) Loop Contribution

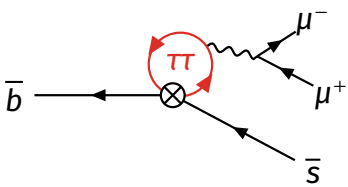

$\tau^+\tau^-$ Loop Contribution

- Another decay contribution is the rescattering tau loop: $B^+ \to K^+(\tau^+\tau^- \to)\mu^+\mu^-$
  - Parameter C_9^τ is expected to be incredibly sensitive to some NP models [PRL 18 (2018)].
- Modelled by adding a further dispersion term to $C_9^{\text{eff}}(q^2)$ [EPJC 12 (2020)].
  - Expected statistical uncertainty on C_9^τ is $\mathcal{O}(< 100)$.
- Viability of fit was investigated in run $1 + 2$, but:
  - Lack of data meant a joint δ_r and η_r had to be used for all 3 2P states.
  - This adds an enormous systematic uncertainty to $C_9^\tau \to$ measurement unviable.
- Will re-attempt a C_9^τ measurement at run 3.

Angular Dimension

- Biggest change is the addition of the angular dimension: $d\Gamma/dq^2 \rightarrow d^2\Gamma/dq^2 d\cos_\mu$
  - Helicity angle $\cos\theta_\mu = \left(\frac{\boldsymbol{p}_B \cdot \boldsymbol{p}_{\mu^-}}{|\boldsymbol{p}_B||\boldsymbol{p}_{\mu^-}|}\right)_{\mu\mu \text{ rest frame}}$
- WCs with different J-number have distinct shapes in non-zero $\cos\theta_\mu$ orders:
  - This protects the fit uncertainties on C_9, C_{10} from exploding.
  - Degeneracies are further broken by interference terms in $\sim\cos\theta_\mu$, $\sim\cos^2\theta_\mu$.

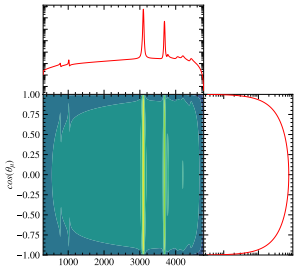

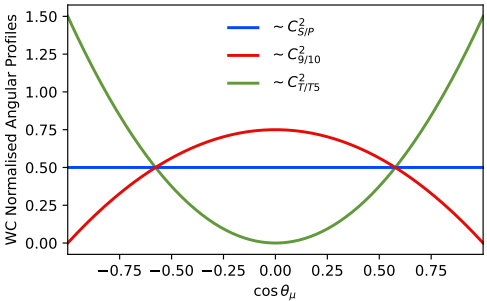

Left: SM-valued PDF visualisation in the $m_{\mu\mu}, \cos\theta_\mu$ plane. Right: Angular profiles of $d\Gamma/d\cos\theta_\mu$, under assumption of only one non-zero WC, as a demonstration of fit-degeneracy breaking angular structure.

Toy Studies

- Toy studies have supported the idea that adding floating WCs does not weaken C_V, C_A fitting ability.
  - ✔ Toys are stable.
  - ✔ Correlations seen in other WCs are all far smaller than those between $C_9 - C_{10}$.
  - ✔ Pull and fit value distributions are consistent with those in C_9, C_{10} only fits.
  - ▶ Will also introduce extra phases to this fit.
  - ▶ Some optimisation remains in fitting procedure.

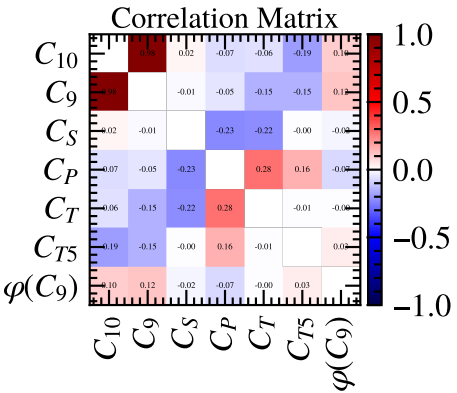

Combinatorial Background

- Run 3 features more combinatorial background.
- Combinatorial needs to be modelled in $m_{\mu\mu}, \cos\theta_\mu$.
  - Unable to just translate UMSB shape due to $\mathcal{R}$ constraint.
  - An ML approach is used to generate the signal region PDF, having trained on UMSB data.
- Tests on pseudodata has shown strong performance.
  - Pseudodata generated from run 1 + 2 analytic combinatorial model.
  - Will be tested + tuned on the fully combinatorial $B^+ \to K^+\mu^+\mu^+$ data channel.

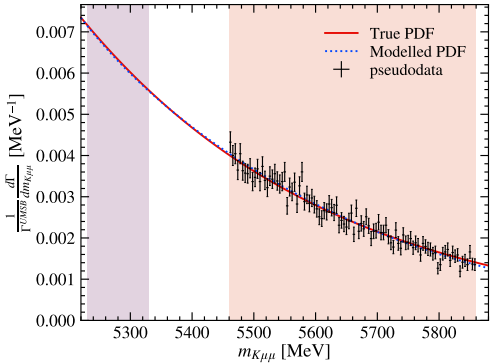

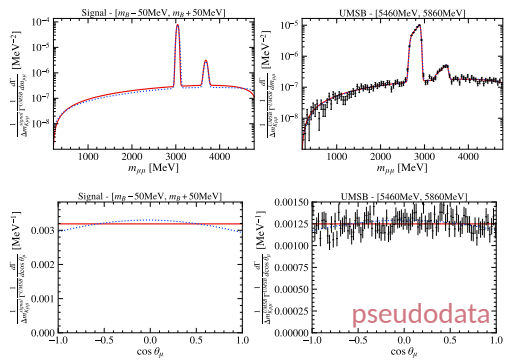

Chapters

Conclusions

- $B^+ \to K^+\mu\mu$ data from runs 1 + 2 at LHCb has been fit using an unbinned model in q^2, with a dispersion model used to incorporate non-locals.
- With the latest HPQCD FFs [PRD 1 (2023)], the C_V, C_A couplings show a SM tension of 4σ.
- When assuming SM-valued C_9' and $C_{10}^{(\prime)}$, measured C_9 is compatible with global $b \to s\mu\mu$ analyses [JHEP 9 (2022)].

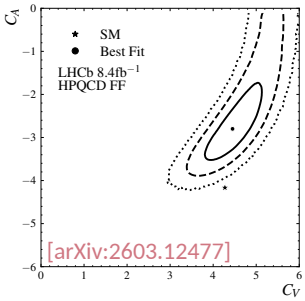

- Run 3 analysis is well positioned to:
  - Improve statistical accuracy on C_V, C_A.
  - Expand number of simultaneously measured WCs.
  - Potentially measure C_9^τ.

Zenodo Link:
doi.org/10.5281/zenodo.19497184

Thanks for listening!

References

[PRD 5 (2016)] J. Gratrex, M. Hopfer and R. Zwicky, *Phys. Rev. D* **93** (2016), 054008, http://dx.doi.org/10.1103/PhysRevD.93.054008

[EPJC 5 (2024)] M. Bordone, G. Isidori, S. Mächler and A. Tinari, *Eur Phys J C.* **84** (2024), 547, http://dx.doi.org/10.1140/epjc/s10052-024-12869-5

[JHEP 4 (2017)] A. Paul and D. M. Straub, *J High Energy Phys* **2017** (2017), 27, http://dx.doi.org/10.1007/JHEP04(2017)027

[PRD 1 (2023)] W. G. Parrott, C. Bouchard and C. T. H. Davies, *Phys. Rev. D* **107** (2023), 014510, http://dx.doi.org/10.1103/PhysRevD.107.014510

[PRD 2 (2016)] J. A. Bailey et al., *Phys. Rev. D* **93** (2016), 025026, http://dx.doi.org/10.1103/PhysRevD.93.025026

[EPJC 12 (2020)] C. Cornella et al., *Eur Phys J C.* **80** (2020), 1095, http://dx.doi.org/10.1140/epjc/s10052-020-08674-5

[JHEP 5 (2025)] LHCb Collaboration, *J High Energy Physics* **2025** (2025), 208, http://dx.doi.org/10.1007/JHEP05(2025)208

[PRL 1 (2020)] LHCb Collaboration, *Phys. Rev. Lett.* **125** (2020), http://dx.doi.org/10.1103/PhysRevLett.125.011802

[arXiv:2603.12477] LHCb Collaboration, *Measurements of the Local and Non-Local Amplitudes in* $B^{\pm} \to K^{\pm}\mu^{\pm}\mu^{\mp}$ *Decays*, Arxiv, 2026

[ANA-2023-016] M. Lakshan et al., *Measurements of the Local and Non-Local Contributions in* $B^{\pm} \to K^{\pm}\mu^{\pm}\mu^{\mp}$ *with Run 1 and Run 2 Data*, CERN-LHCb-ANA-2023-016, 2013

[EPJC 3 (2017)] LHCb Collaboration, *Eur Phys J C.* **77** (2017), 161, http://dx.doi.org/10.1140/epjc/s10052-017-4703-2

[JHEP 6 (2014)] LHCb Collaboration, *J High Energy Phys* **2014** (2014), 133, http://dx.doi.org/10.1007/JHEP06(2014)133

[JHEP 9 (2022)] N. Gubernari, M. Reboud, D. van Dyk and J. Virto, *J High Energy Phys* **2022** (2022), 133, http://dx.doi.org/10.1007/JHEP09(2022)133

[arXiv:2603.12477] LHCb collaboration, *Differential decay rate of* $B^{+} \to J/\psi K^{+}$ *with the LHCb Upgrade I experiment*, Arxiv, 2026

[lhcb-outreach.web.cern.ch] B. Pietrzyk, *End of the 2025 Proton-Proton Collision Run*, `https://lhcb-outreach.web.cern.ch/2025/11/11/end-of-the-2025-proton-proton-collision-run/`, Accessed: 2026-04-13

[cds.cern.ch/record/2950664] LHCb Collaboration, *End of the 2025 Proton-Proton Collision Run*, `https://cds.cern.ch/record/2950664`

[PRL 18 (2018)] B. Capdevila et al., *Phys Rev Lett* **120** (2018), 181802, http://dx.doi.org/10.1103/PhysRevLett.120.181802

[PLB 781 (2018)] CMS Collaboration, *Physics Letters B* **781** (2018), 517, http://dx.doi.org/10.1016/j.physletb.2018.04.030

[PRL 15 (2021)] LHCb Collaboration, *Phys Rev Lett* **127** (2021), 151801, http://dx.doi.org/10.1103/PhysRevLett.127.151801

Backup Slides

EFT in $b \to s\ell\ell$ Decays

- Higher energy physics ($E > m_b$) in $b \to s\ell\ell$ decays is integrated out, producing an effective field theory (EFT) hamiltonian, $\mathcal{H}_{\text{eff}}$:

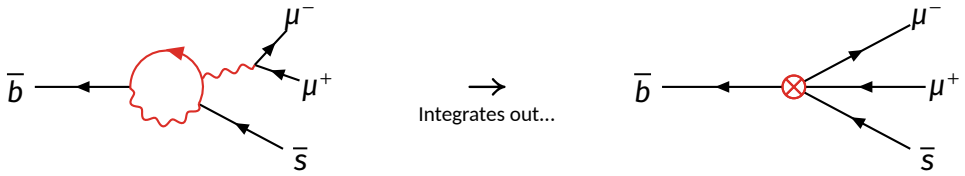

$$\mathcal{A}_{\mathrm{i}\to\mathrm{f}} = \langle \mathrm{f}|\mathcal{H}_{\text{eff}}|\mathrm{i}\rangle = \frac{G_F}{\sqrt{2}} V_{tb}V_{ts}^* \sum_j C_j \langle \mathrm{f}|\mathcal{O}_j|\mathrm{i}\rangle$$

- Long range physics is described by the operators, $\mathcal{O}_j$, with the short range physics summarised by the Wilson Coefficients (WCs), C_j.
  - High energy new physics (NP) will perturb the relevant C_j value away from the standard model (SM) prediction by δC_j^{NP}.

B Flavour Anomalies

- Past measurements of $b \to s\ell\ell$ transitions have persistently shown SM tensions.
  - Observed across a range of observables and detectors.
  - Often observed to be consistent with a $\delta C_9^{NP} < 0$ hypothesis.
- Global fits of the WCs support these observations, with [JHEP 9 (2022)] suggesting $\delta C_9^{NP} \simeq -1.0$, and [EPJC 5 (2024)] fitting for $\delta C_9^{NP} = -1.3 \pm 0.1$.
  - Further, more sensitive, fits of C_9 are strongly motivated.

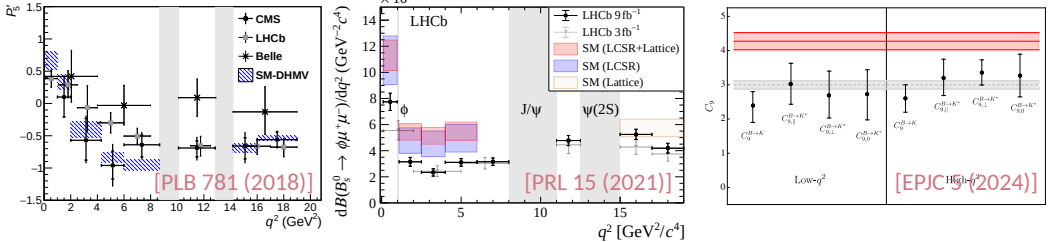

Demonstrative C_9 conducive anomalies in P_5' in $B^0 \to K^{*0}\mu\mu$ decays (left), and in dBF/dq^2 in $B_s^0 \to \phi\mu\mu$ (middle). Right: fit to independent determinations of C_9 in several $B \to K^{(*)}$ decays.

2D WC Fits Incl. Previous Analysis

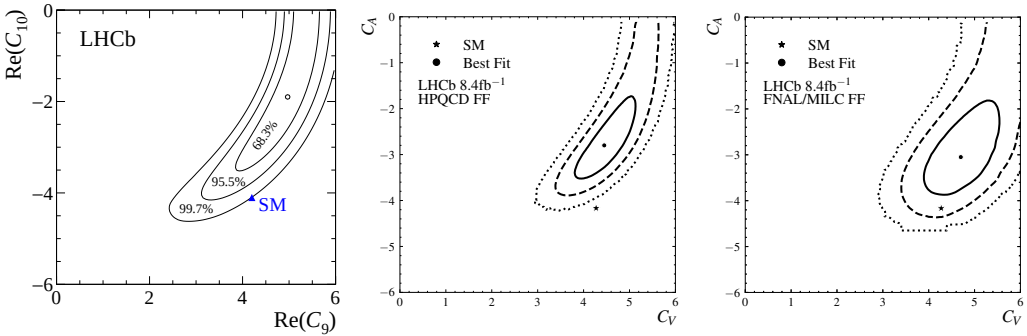

Left: $C_9 - C_{10}$ plane taken from the run 1 analysis: arXiv:1612.06764v2. Middle: $C_9 - C_{10}$ in the current analysis, fitted with the HPQCD form factors. Right: $C_9 - C_{10}$ in the current analysis, fitted with the FNAL/MILC form factors.

Systematic Uncertainties

Systematic uncertainties on the parameters of interest. See https://arxiv.org/abs/2603.12477 for more information.

Parameter	HPQCD FF	$BF(B^+ \to J/\psi K^+)$	Resolution	Bkg extrapolation	Subtraction
C_V	0.141	0.079	0.013	0.012	0.065
C_V	0.084	0.014	0.034	0.031	–
δ_ρ [rad]	0.074	0.002	0.016	0.005	–
η_ρ	0.012	0.001	0.001	0.001	–
δ_ω [rad]	0.006	0.015	0.018	0.001	–
η_ω	0.058	0.005	0.009	0.001	–
$\delta_{\phi(1020)}$ [rad]	0.005	0.051	0.004	0.002	–
$\eta_{\phi(1020)}$	0.082	0.004	0.010	0.001	–
$\delta_{J/\psi}$ [rad]	0.018	0.001	0.002	0.006	–
$\delta_{\psi(2S)}$ [rad]	0.027	0.006	0.006	0.012	–
$\eta_{\psi(2S)}$	41.42	18.69	0.020	0.087	–
$\delta_{\psi(3770)}$ [rad]	0.030	0.002	0.003	0.011	–
$\eta_{\psi(3770)}$	0.099	0.035	0.006	0.040	–
$\delta_{\psi(4040)}$ [rad]	0.098	0.003	0.006	0.018	–
$\eta_{\psi(4040)}$	0.135	0.015	0.009	0.006	–
$\delta_{\psi(4160)}$ [rad]	0.107	0.002	0.007	0.009	–
$\eta_{\psi(4160)}$	0.118	0.023	0.013	0.010	–
$\delta_{\psi(4415)}$ [rad]	0.085	0.002	0.016	0.010	–
$\eta_{\psi(4415)}$	0.072	0.016	0.027	0.009	–
δ_{2P} [rad]	0.207	0.003	0.035	0.017	–
η_{2P}	0.137	0.002	0.005	0.021	–

Helicity Formalism - arXiv:1506.03970

$$\frac{d^2\Gamma}{dq^2 d\cos\theta_\mu} = \mathbb{G}^0 + \mathbb{G}^1 \cos\theta_\mu + \frac{\mathbb{G}^2}{2}\left(3\cos^2\theta_\mu - 1\right)$$

Where:

$$\begin{aligned}
\mathbb{G}^0 &= \frac{4}{3}\left(1 + 2\hat{m}_\ell{}^2\right)|h^V|^2 + \frac{4}{3}\beta_\ell^2|h^A|^2 + 2\beta_\ell^2|h^S|^2 + 2|h^P|^2 + \\
&\quad + \frac{8}{3}\left(1 + 8\hat{m}_\ell{}^2\right)|h^{T_t}|^2 + \frac{4}{3}\beta_\ell^2|h^T|^2 + 16\hat{m}_\ell \mathrm{Im}\left[h^V \bar{h}^{T_t}\right] \\
\mathbb{G}^1 &= -4\beta_\ell\left(2\hat{m}_\ell \mathrm{Re}\left[h^V \bar{h}^S\right] - \mathrm{Im}\left[2h^{T_t}\bar{h}^S + \sqrt{2}h^T\bar{h}^P\right]\right) \\
\mathbb{G}^2 &= -\frac{4\beta_\ell^2}{3}\left(|h^V|^2 + |h^A|^2 - 2|h^T|^2 - 4|h^{T_t}|^2\right)
\end{aligned}$$

Helicity Formalism - arXiv:1506.03970

Note: Notation displayed here is consistent with the rest of this presentation, and is distinct from that used in arXiv:1506.03970.

$$h^S = \frac{m_B^2 - m_K^2}{2}\left(\frac{C_S + C_S'}{m_b - m_s}\right) f_0$$

$$h^P = \frac{m_B^2 - m_K^2}{2}\left(\frac{C_P + C_P'}{m_b - m_s} + \frac{2m_\mu\,(C_A + C_A')}{q^2}\right) f_0$$

$$h^V = \frac{\sqrt{\lambda_{BK}}}{2\sqrt{q^2}}\left(\frac{2m_b}{m_B + m_K}\left(C_7^{\text{eff}} + C_7'\right) f_T + C_V f_+\right)$$

$$h^A = \frac{\sqrt{\lambda_{BK}}}{2\sqrt{q^2}} C_A f_+$$

$$h^T = -i\frac{\sqrt{\lambda_{BK}}}{2\,(m_B + m_K)} C_{T5} f_T$$

$$h^{T_t} = -i\frac{\sqrt{\lambda_{BK}}}{2\,(m_B + m_K)} C_T f_T$$

$$h^X \equiv \langle \overline{K}|\overline{s}\overline{\Gamma}^X b|\overline{B}\rangle$$

The LHCb Detector in Runs 1 + 2

- Specialised B detector at the LHC. In a symmetric $p-p$ environment.
  - Substantially higher statistics than B-factories $\left(\mathcal{O}(10^{12})\ b\bar{b}\text{ pairs produced per year}\right)$.
  - Much messier environment.
- b hadrons produced with p ~ 80GeV
  - Decay time of ~ 3×10^{-11}s.
  - Decay length of ~ 7mm.

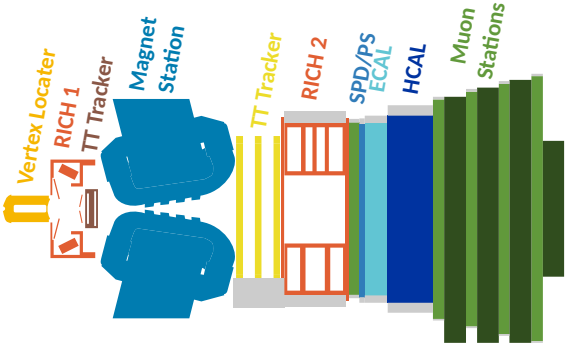

Run 1 + 2 Performance Summaries:

- $\frac{\delta p}{p} = 0.5-1.0\%$ while $p \in [20, 200]$GeV
- $\frac{\delta E}{E}\ (\text{ECAL}) = 1\% + \frac{10\%}{\sqrt{E/\text{GeV}}}$
- $\frac{\delta E}{E}\ (\text{HCAL}) = 9\% + \frac{69\%}{\sqrt{E/\text{GeV}}}$
- $\delta IP = 15\mu\text{m} + \frac{29}{p_T/\text{GeV}}\mu\text{m}$

Modelled Backgrounds - $\pi \to K$ mis-ID

- $B^+ \to \pi^+\mu\mu$ closely kinematically mimics $B^+ \to K^+\mu\mu$.
  - Primary handle is information from the RICH PID system on mass estimation.
  - Still see about mis-ID/signal rate of ~10^{-3}.
- Modelled with a kernel density estimator.
  - Trained using simulated data corrected by comparison to high-purity data channels.
  - Performed separately for run 1 + 2, then summed.

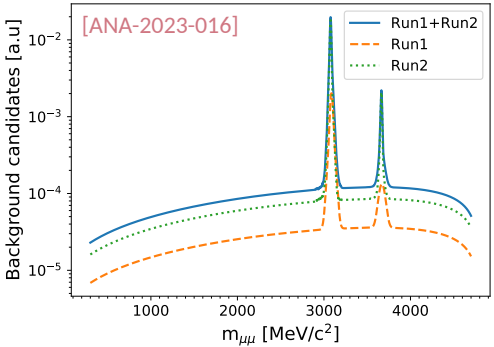

Combinatorial Background - Method

- Combinatorial background is has 3 distinct contributions: broad, J/ψ , and $\psi(2S)$.
  - Incredibly different scales and shapes, ML models struggle to capture all 3 simultaneously.
- Train 3 neaural networks over different phase space regions:
  - Broad combinatorial NN, blind to J/ψ and $\psi(2S)$ regions.
  - J/ψ and $\psi(2S)$ NNs, trained to 'make up the difference' in these regions.
- Trained on linearly transformed, reweighted pseudodata to make phase space division more convenient.